Development of an Integrated Urban Heat Island Simulation Tool

Ming Xu

Future Cities Laboratory, Singapore-ETH Centre, ETH Zurich

*Corresponding Author: Ming Xu, Future Cities Laboratory, Singapore-ETH Centre, ETH Zurich

ABSTRACT

Urban heat island (UHI) effect is quite common in megacities due to the built-up area and reduced greenery coverage of land surface, which highly affect urban livability. An integrated urban heat island simulation tool is developed by accounting for major heat sources and heat sinks in selected area of interest, and their interactions with the surrounding environment. Validation of simulated solar radiation and air temperature is conducted at Kent Vale buildings and Punggol Waterway Terrace I, with correlation coefficient (r) of 0.98 and 0.90, and mean absolute error (MAE(%)) of 4% and 13%, respectively. The validation results confirm the performance of the simulation tool. As an implementation example of the developed integrated urban heat island simulation tool, effects of air conditioners, traffic, grasslands and water bodies on urban thermal environment are investigated by comparing results from two different scenarios, namely the base scenario where all regions are set as concrete and the real situation scenario where each region is set as its own property. It is found that (1) the simulation tool is able to simulate the stack effects induced by split-type air conditioners accurately; (2) the air temperature above Clementi Road is more than 2 ℃ higher than surrounding air throughout the daytime except during the early morning and can affect air even at 8m above the ground; (3) grasslands can cool down much larger area than their upright surface with capability of around 2 ℃ decided by the size of grassland through intrusion into the hotter regions from gaps between three high-rise buildings and the verandah; (4) the air temperature at the water surface of the swimming pool is found to be around 1.5 ℃ cooler than the surrounding air and can go up to 1m above the water surface with temperature of around 0.5 ℃ lower than the surrounding air.

Keywords: *Urban heat island effect, Integrated simulation tool, Effects of air conditioners, Effects of traffic, Effects of grasslands, Effects of water bodies;*

INTRODUCTION

Urban heat island (UHI) effect is described as the phenomenon that the air temperature in urban area is consistently higher than its rural area (Oke, 1973). While many causes of the urban heat island such as reduced evaporation, increased heat storage, increased net radiation, reduced convection and increased anthropogenic heat have been identified as in Gartland (2008), the contribution of each component strongly depends on the individual city and its geography. In a high-density mixed-used tropical city like Singapore, the urban microclimate varies from location to location and time to time.

From previous research, we have a broad understanding of the magnitude of the urban heat island effect in Singapore, and of its main causes. A study of air temperatures conducted in

Wong and Chen (2006) between2001-2004 showed that the UHI intensity in Singapore was about 4.5° C. Another study from Chow and Roth (2006) found that the peak UHI magnitude occurs approximately six hours after sunset at central business districts, high-rise residential estate, and low-rise residential area. Higher UHI intensities generally occur during the southwest monsoon period of May–August, with a maximum of ~7° C observed at Orchard Road at approximately 21:00 local time (Chow and Roth, 2006).More detailed information about the influence of albedo on the UHI in Singapore has been obtained from satellite or aerial images (Mackey et al., 2012). Wong and Chen (2006) concluded that hotspots are normally observed in the urban context on exposed hard surfaces during the daytime, and suggested that these could be addressed through shading by greenery or artificial sun-shading devices. Several other

studies have investigated the urban microclimate in Singapore relating to the urban heat island effect (Chow et al., 2014; Shaffer et al., 2014; Roth and Chow, 2012; Jusuf et al., 2007; Chow and Roth, 2006; Li et al., 2013). Research exists on several counter-measures, such as rooftop gardens and albedo (Sproul et al., 2014; Gao et al., 2014; Chen and Wong, 2006; Li and Norford, 2016).

Recent challenges in modeling of urban heat island are reviewed in Mirzaei (2015) by addressing problems in building-scale models, micro-scale models and city-scale models. It is concluded that microclimate and building models cannot cover the entire city due to the complex parameters and extensive computational cost. Despite the capability of mesoscale models in investigation of the large-scale UHI effect, their accuracy is not sufficient to provide detailed information of the urban canopy layer. This gap requires further research to develop computationally and spatially efficient models. Urban heat island is a typical multi-physics multi-scale problem, which calls for integrated evaluation of the complex interactions between each key component in the system. As pointed out in Xu (2016), it is necessary to quantify the respective effects of major heat sources and sinks which contribute to urban heat island effect in Singapore. Xu (2016) concludes that solar radiation is the predominant heat source in Singapore, whose effects and interactions with buildings and surrounding air is investigated in Xu et al. (2017). Other heat sources contribute to urban heat island effect is mainly induced by anthropogenic activities Quah and Roth (2012), such as industrial activities, building energy consumption and traffic system. Major heat sinks in the urban context are grasslands, trees and water bodies.

To account for the combined effects of different heat sources and sinks with various physics background, model coupling is a widely adopted and well proven numerical technique. For instance, to simulate the combined effects of building energy consumption and the surrounding environment, coupled building energy consumption and environment models are implemented in Allegrini et al. (2015) and Allegrini and Carmeliet (2017) by coupling the Computational Fluid Dynamic (CFD) model with radiation model. To simulate cooling effects from heat sinks through evaporation such as water bodies, coupled CFD and radiation models are also widely used (Saneinejad et al.,

2012; Tominaga et al., 2015). Cooling effects of greenery including grasslands and trees could be modeled as porous media with the coupled CFD and radiation model by adding source terms to the governing equations, as adopted in Saneinejad et al. (2012). Various modeling tools and systems are developed across the world to manage and evaluate the impacts of different urban elements and urban designs on urban heat island effect in city-scale and outdoor thermal comfort in neighborhood-scale and street- scale. Assessment of tools developed in Japan for urban climate is conducted in Ooka (2007) by classifying them according to corresponding modeling scales. It is shown that these assessment tools are quite powerful in estimating countermeasures of urban heat island effect and could be implemented as design tools for practical applications. An operational modeling system for urban heat island effect is developed and implemented to Athens, Greece, as reported in Giannaros et al. (2014). The modeling system is built on the basis of a state-of-art numerical weather prediction model which is properly modified to allow for better representation of the urban climate. While few modeling tools account for the integration of major heat sources including solar radiation, industrial activities, building energy consumption and traffic system, and major heat sinks including grasslands, trees and water bodies are developed.

The main objective of this study is to develop an integrated urban heat island simulation tool by accounting for major heat sources and heat sinks in selected area of interest, and their interactions with the surrounding environment. This paper is structured as follows: Section 2 presents methodology applied in this study, Section 3 shows the validation process of the developed integrated simulation tool, Section 4 illustrates the results and related discussions, Section 5 draws conclusions of this study.

METHODS

Three universal conservation laws of mass, momentum and energy are taken into account by solving continuity equation (Equation (1)), Navier-Stokers equation (Equation (2)) and energy balance equation (Equation (3)). The flow field and the transport phenomena developed in the

computational domain are described by the Reynolds Averaged Navier-Stokes (RANS) equations. The continuity, momentum and energy conservation equations are solved in a 3D (x, y, z) domain, as well as the equations correspond to the turbulence model. Conjugate heat transfer is simulated by solving heat convection (Equation (4)), conduction (Equation (5)) and radiation (Equation (6)) between fluid and solid regions. The turbulence effect in the developed flow and heat transfer is modeled through the standard $k − ε$ model.

$$\frac{\partial \rho}{\partial t} + \nabla \cdot (\rho u) = 0 \tag{1}$$

$$\frac{\partial (\rho u)}{\partial t} + \nabla \cdot (\rho u \otimes u + pI) = \mu \nabla^2 u + \rho g \tag{2}$$

$$\rho C_p \left(\frac{\partial T}{\partial t} + u \cdot \nabla T \right) = \kappa \nabla^2 T + Q \tag{3}$$

$$q = h(T_a - T_\infty) \tag{4}$$

$$q = -k \nabla T \tag{5}$$

$$q = \epsilon \sigma (T_a^4 - T_b^4) \tag{6}$$

where ρ is density, t is time, u is flow velocity field, p is pressure, I is the identity matrix, μ is turbulent eddy viscosity, g is the gravity acceleration rate, T is temperature, C_p is the specific heat, κ is the thermal conductivity, Q is the additional heat flux, h is the heat transfer coefficient, ϵ is the radiation factor and σ is the Stefan-Boltzmann constant, respectively.

Solar radiation is simulated by accounting for the combined effects of the Sun primary hits, their reflective fluxes and diffusive sky radiative fluxes (Howell et al. 2010). The primary hit rays of solar radiation are calculated using a face shading algorithm. The reflected fluxes are considered diffusive and use a view factors method to deposit the energy on visible walls. The sky diffusive radiation for horizontal and vertical walls is calculated following the Fair Weather Conditions Method from the ASHRAE Handbook.

Ray tracing technique of the solar load model is used to forecast the direct illumination energy source induced by incident solar radiation. By using the illumination parameters and the sun position vector, a beam is applied to any faces to carry out a face-by-face shading analysis to compute the heat flux on the boundary faces that results from the incident radiation and determine shadows on all interior walls and boundary faces. The resulting heat flux computed by the solar

ray tracing algorithm will be coupled to the energy equation with a source term. The heat sources are assigned to adjacent cells such as solid cells, shell conduction cells, and fluid cells and added to computational cells which are bordering each face. A two-band spectral model which accounts for different material properties in the infrared and visible bands is used for direct solar illumination. Diffuse radiation is calculated by a hemispherical-averaged single-band spectral model. Opaque materials are characterized by two-band absorptive. The shading calculation used for solar ray tracing is a straightforward vector geometry calculation. A ray is traced from the face centroid in the sun direction. Every other face is checked to determine if the candidate face is in front of the target face and if the ray intersects the target face. An opaque face completely shades the test face if both requirements are met.

A solar calculator is designed to compute solar beam directions and irradiation for a given time, date and position consists of latitude and longitude. These values can be used as inputs to the solar ray tracing algorithms. The equation for normal direct irradiation applying the Fair Weather Conditions Method is taken from the ASHRAE Handbook:

$$Edn = \frac{A}{e^{\frac{B}{\sin \beta}}} \tag{7}$$

where A and B are apparent solar radiation at air mass $m = 0$ and atmospheric extinction coefficient, respectively. These values of A and B are based on the earth's surface on a clear day. β is the solar altitude (in degrees) above the horizon. This algorithm is also similar to the solar calculator adopted in ANSYS FLUENT.

The greeneries including grasslands and trees are considered as heat sinks and porous materials that cause pressure drop. In the momentum conservation equations two source terms are added, which correspond to the thermal buoyancy and the pressure drop inside the porous media, as presented in Fidaros et al. (2017).

Six extra terms are added in the energy equation, which are a source term corresponding to thermal radiation calculated by the solar load model, three more source terms corresponding to the heat produced by buildings, traffic system and industrial activities and two sink terms that correspond to the air temperature reduction due to evapotranspiration and evaporation of greenery and water bodies, respectively. Other

model set up follows strictly the suggestions made in Xu (2017).

Open FOAM (www.openfoam.com) is implemented in this study as the core model, which is a free and open source Computational Fluid Dynamics (CFD) software developed primarily by Open CFD Ltd since 2004 and distributed by Open CFD Ltd and the Open FOAM Foundation. The non-uniform thermal boundary condition was defined by considering the solar irradiance that enables to include the effect of shading and solar heating. Docker (www.docker.com) is employed to perform parallel computing on the 128-core High Performance Computer (HPC) in Future Cities Laboratory of Singapore-ETH Centre. Parallel computing together with the customized CFD program coupled with solar radiation model and other key components to simulate conjugate heat transfer ensured the high-performance of this tool in terms of both accuracy and efficiency.

MODEL VALIDATION

To validate the performance of the developed integrated urban heat island simulation tool, two rounds of simulations are carried out and compared against observed data after calibrating the key parameters of the tool. In the first round, Kent Vale buildings (Figure 1), which are the housing unit of faculty members of National University of Singapore, are chosen. The location of the Kent Vale buildings, which is the key input information of the earlier developed solar radiation model as one of the tool forcing, is (1.302°N, 103.768°E) in latitude and longitude, respectively. The model domain for Kent Vale Buildings is selected as 250m ×250m× 200m in x, y and z directions, respectively. With snappyHexMesh of Open FOAM, a high resolution of around 5cm is achieved for the smallest edges of buildings and the total number of cells is 1.27 million. Different regions are identified in Figure 1, including buildings, greeneries, road pavement and water bodies. Thermo physical and radiation properties of different materials involved in both

models are set as tabulated in Table 1. Key parameters are molar weight of the substance (mol Weight) in kg/mol, specific heat capacity (Cp) in J/kg•K, dynamic viscosity (mu) in Pa•s, Prandtl number (Pr), thermal conductivity (Kappa) in W/m•K, density of the material (Density) in kg/m3 and emissivity, absorptive, transmissivity and reflectivity of different materials. Solar radiation is calculated with the coupled solar load model by setting the specific date of the typical day during each month and location of the Kent Vale buildings. The tool is forced by the real settings of initial air temperature and velocity of each split type air-conditioners on both sides of the Kent Vale buildings, as measured in Bruelisauer et al. (2014). Time series of heat flux due to traffic system from 6am to 8pm during daytime (Figure 2) is adopted after part of Figure 3 in Quah and Roth (2012), which is employed as the forcing of traffic heat flux in the simulation tool. The cooling effects of greeneries are simulated by regarding the porous media which represent grasslands as heat sinks by assuming the cooling power of the grasslands is 22.5 W/m2, as reported in Edwards et al. (2016) for evaporative cooling power of a typical rain tree in Singapore. A close cooling power of 20 W/m2is also set for the water bodies involved in the model domain, with reference values from Fidaros et al. (2017). The initial air temperature is set as 27°C in the early morning at 6am as provided by the measured data from the nearest meteorological station of National Environmental Agency (NEA). Wind profile on each specific date is set according to the measured data at the meteorological station at National University of Singapore, which is around 500m from the center of the model domain, as one of the boundary conditions. Other boundary and initial conditions include turbulent dissipation rate ε, turbulent kinetic energy k, kinematic turbulence viscosity ν_t, pressure p, wall function parameter α and incident radiation intensity G, which are calculated according to the real situations of the environment around Kent Vale buildings.
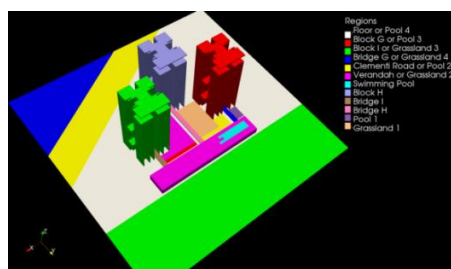

Figure1. *3D geometriesof Kent Vale buildings with different regions identified.*

Table1. *Thermo physical and radiation properties of different materials.*

	Air	Concrete	Water
molWeight (kg/mol)	28.97	200	18
Cp (J/kg•K)	1004	750	4180
mu (Pa•s)	0.000018	-	0.001057
Pr	0.7130	-	6.5241
Kappa (W/m•K)	-	0.8	-
Density (kg/m³)	-	2240	1000
Emissivity	-	0.7	0.1
Absorptivity	-	0.7	0.1
Transmissivity	-	0	0.4
Reflectivity	-	0.3	0.5
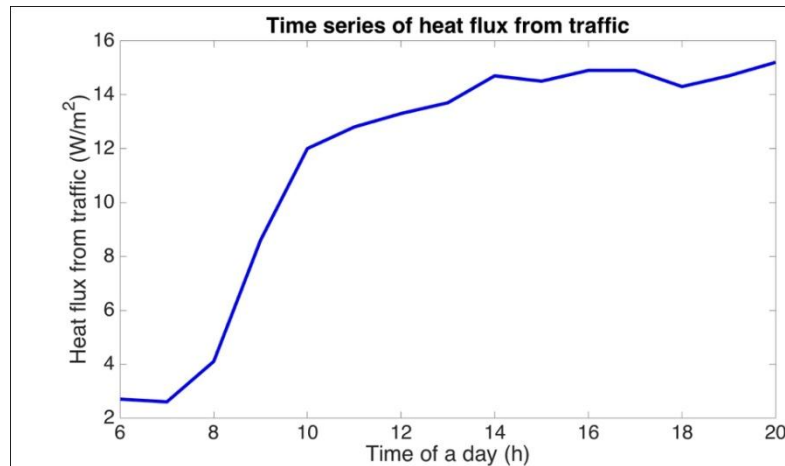
Figure2. *Time series of heat flux from traffic on Clementi Road. Regenerated after part of Figure 3 in Quah and Roth (2012).*

Simulated solar radiation and air temperature on a typical day of each month are validated against observed data provided by National University of Singapore Meteorological Station (Figures 3-4, Tables 2-3). Statistical evaluations are performed by calculating the correlation coefficient (r) and the mean absolute error in percentage (MAE (%)).

$$r = \frac{\sum(X_{model} - \overline{X_{model}})(X_{obs} - \overline{X_{obs}})}{\sqrt{\sum(X_{model} - \overline{X_{model}})^2 \sum(X_{obs} - \overline{X_{obs}})^2}} \tag{8}$$

$$MAE \, (\%) = \frac{\sum|(X_{model} - X_{obs})|}{(max(X_{obs}) - min(X_{obs}))N} \tag{9}$$

where X_{model} and X_{obs} are simulated and observed quantity, respectively. $\overline{X_{model}}$ and $\overline{X_{obs}}$ are the mea values of simulated and observed quantities, respectively. N is the total number of quantities involved in the calculation. $max(X_{obs})$ and $min(X_{obs})$ are the maximum and minimum observed data among all involved quantities in the calculation, respectively. The calculation of observed solar radiation in each month throughout the whole year around Kent Vale buildings can be found in Xu (2016).

It is found that the simulated radiation (Figure 3) and air temperature (Figure 4) generally agree well with observations, with r of 0.99, 0.98 and MAE (%) of 2%, 4%, respectively (Tables 2 and 3). This shows that the modeling developed integrated urban heat island simulation tool could capture most portion of solar radiation and air temperature. Much smaller solar radiation and lower air temperature in November and December are observed due to the heavy rainfall during the Northeast monsoon season. Heavy rainfall will diffuse more solar radiation, enhance evaporation of water on the group which low down the air temperature.
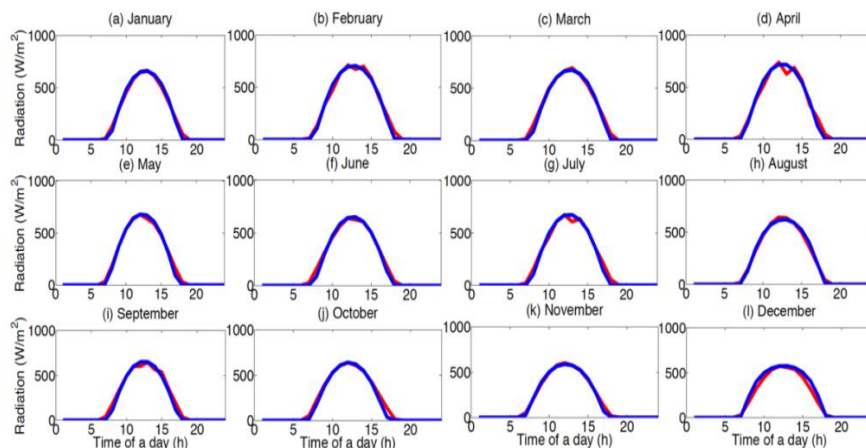
Figure3. *Validated solar radiation on a typical day of each month against measured data. Legend: measured data (red line), simulated results (blue line).*
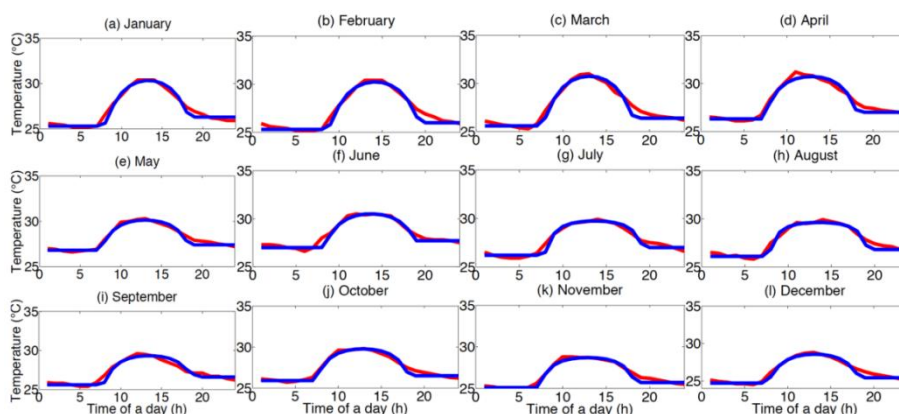
Figure4. *Validated air temperature on a typical day of each month against measured data. Legend: measured data (red line), simulated results (blue line).*

Table2. *Statistics of simulated solar radiation on a typical day of each month.*

	Jan	**Feb**	**Mar**	**Apr**	**May**	**Jun**	**Jul**	**Aug**	**Sep**	**Oct**	**Nov**	**Dec**
r	0.99	0.99	0.99	0.99	0.99	0.99	0.99	0.99	0.99	0.99	0.99	0.99
MAE(%)	1.67	1.97	1.66	2.48	1.55	1.78	2.02	1.78	1.72	1.40	1.39	1.22

Table3. *Statistics of simulated air temperature on a typical day of each month.*

|	**Jan**	**Feb**	**Mar**	**Apr**	**May**	**Jun**	**Jul**	**Aug**	**Sep**	**Oct**	**Nov**	**Dec**
r	0.98	0.99	0.98	0.98	0.98	0.98	0.98	0.98	0.97	0.98	0.99	0.98
MAE(%)	4.96	5.11	4.96	5.02	5.03	4.94	5.59	5.79	6.59	5.24	5.11	5.63

To further evaluate the performance of the developed simulation tool in simulating air temperature, Punggol Waterway Terrace I (Figure 5) is chosen as the second site to compare the simulated results with observed data measured by 49 sensors deployed on-site on 6 Feb 2017. The location of Punggol Waterway Terrace I is (1.408°N, 103.900°E) in latitude and longitude, respectively. Similar settings to the first case of Kent Vale buildings are made by identifying different regions including buildings and greeneries. As shown in Figures 6-11, the simulated time series of air temperature at 49 sensors generally match well with observed data, with slight overestimations at Sensors 17-22 especially during noon time. The discrepancies at Sensors 17-22 are mainly due to the underestimation of the cooling power of surrounding greeneries, which has a dynamic performance throughout the whole day

especially the peak values during noon time. To improve the model accuracy in predicting air temperature at a complex situation as Sensors 17-22, detailed measurements of cooling power of surrounding trees and grasslands are needed, especially the dynamic performance throughout the whole day. A great sample study of such measurements is presented in Tan et al.

(2017).According to Table 4, the correlation coefficient r is consistently larger than 0.90 and the MAE(%) is around 13%, which indicates that the developed integrated urban heat island simulation tool could simulate quite accurate air temperature around real buildings with detailed information.
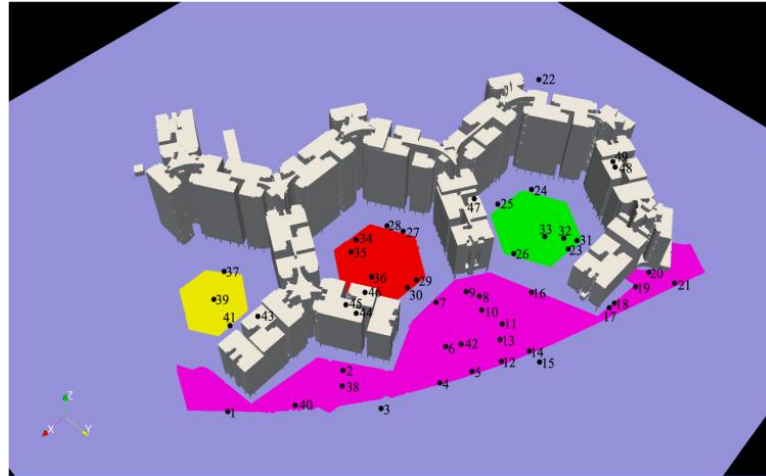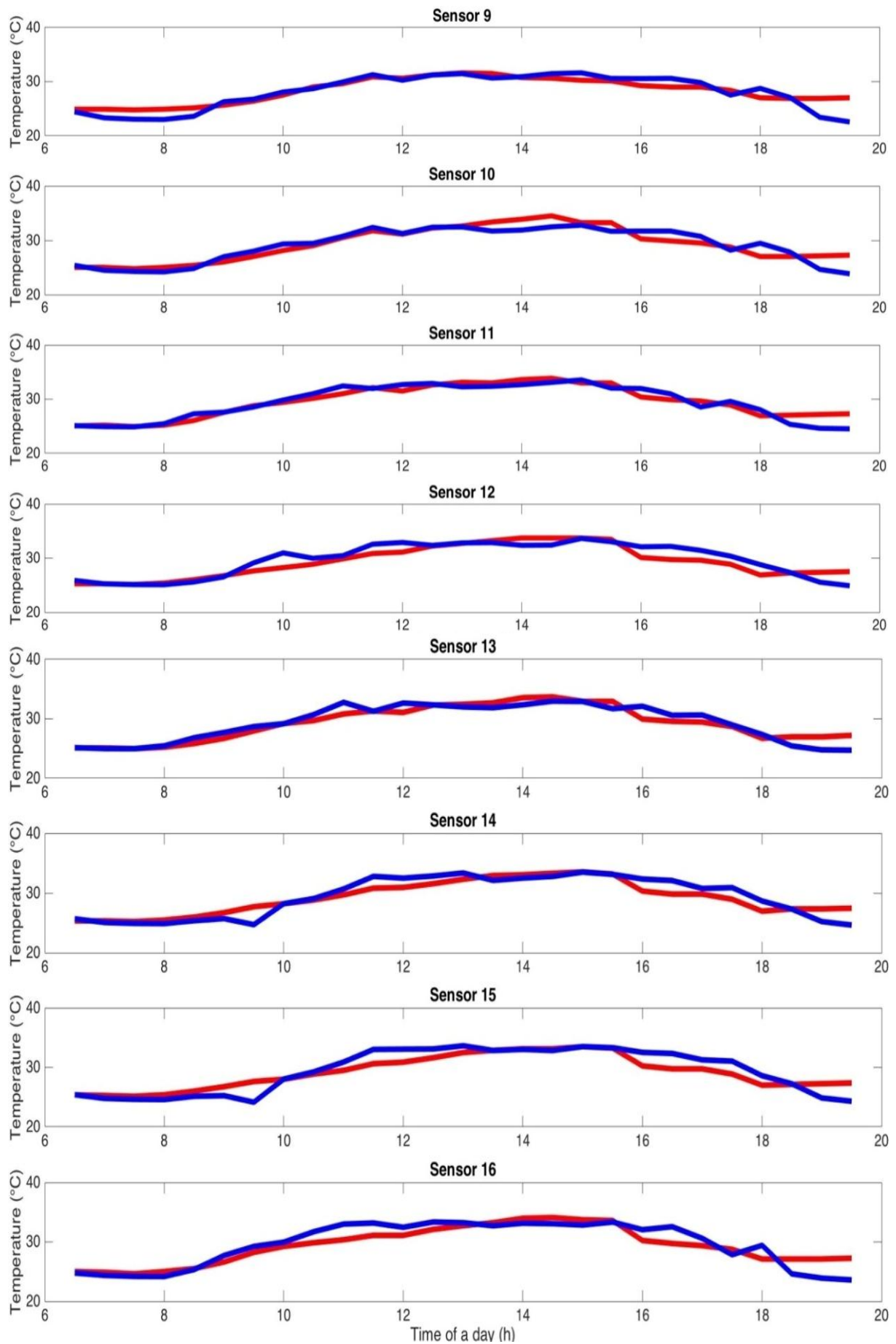

Figure5. *3D geometries of Punggol Waterway Terrace I and the 49 deployed sensors.*
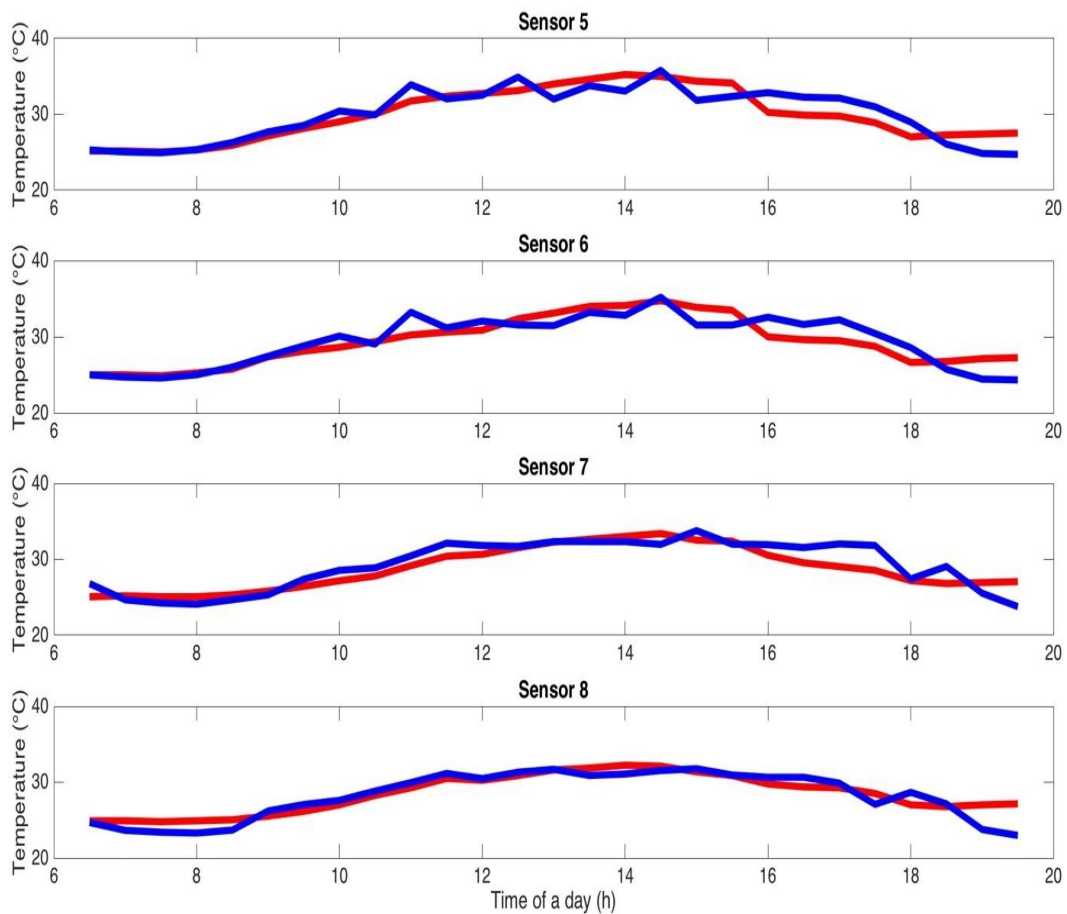
Figure6. *Validated air temperature at Sensors 1-8 against measured data. Legend: measured data (red line), simulated results (blue line).*
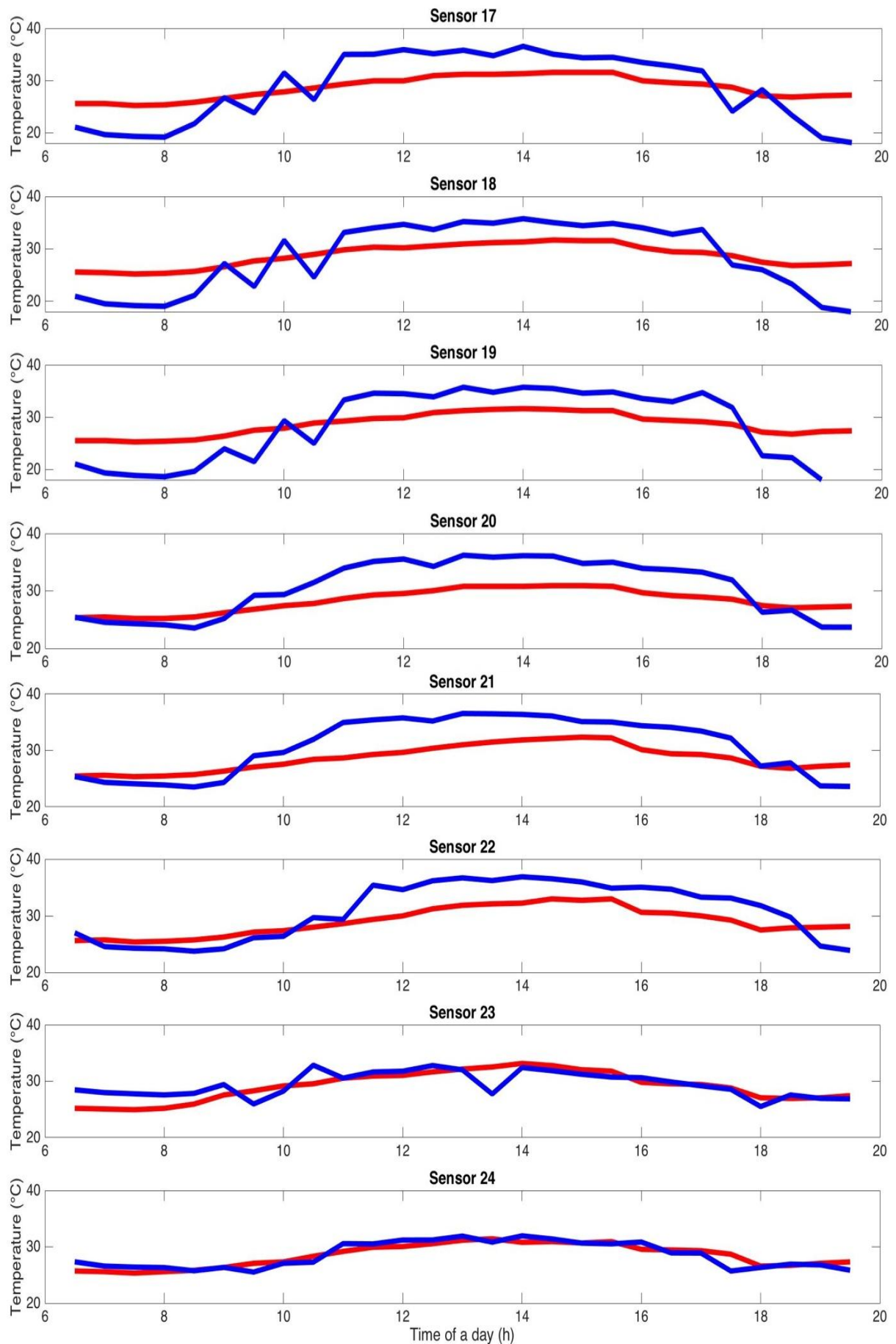
Figure7. Validated air temperature at Sensors 9-16 against measured data. Legend: measured data (red line), simulated results (blue line).
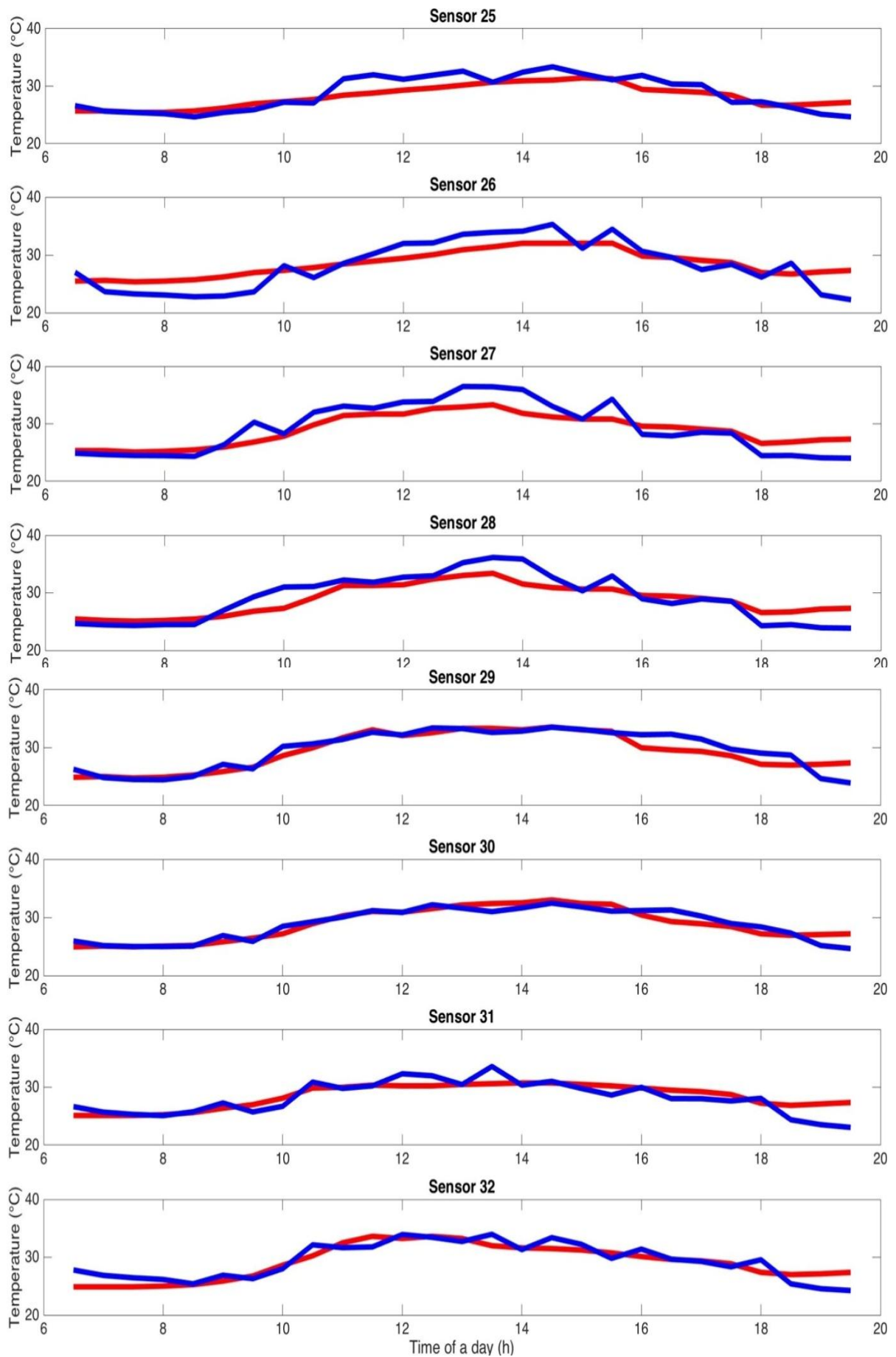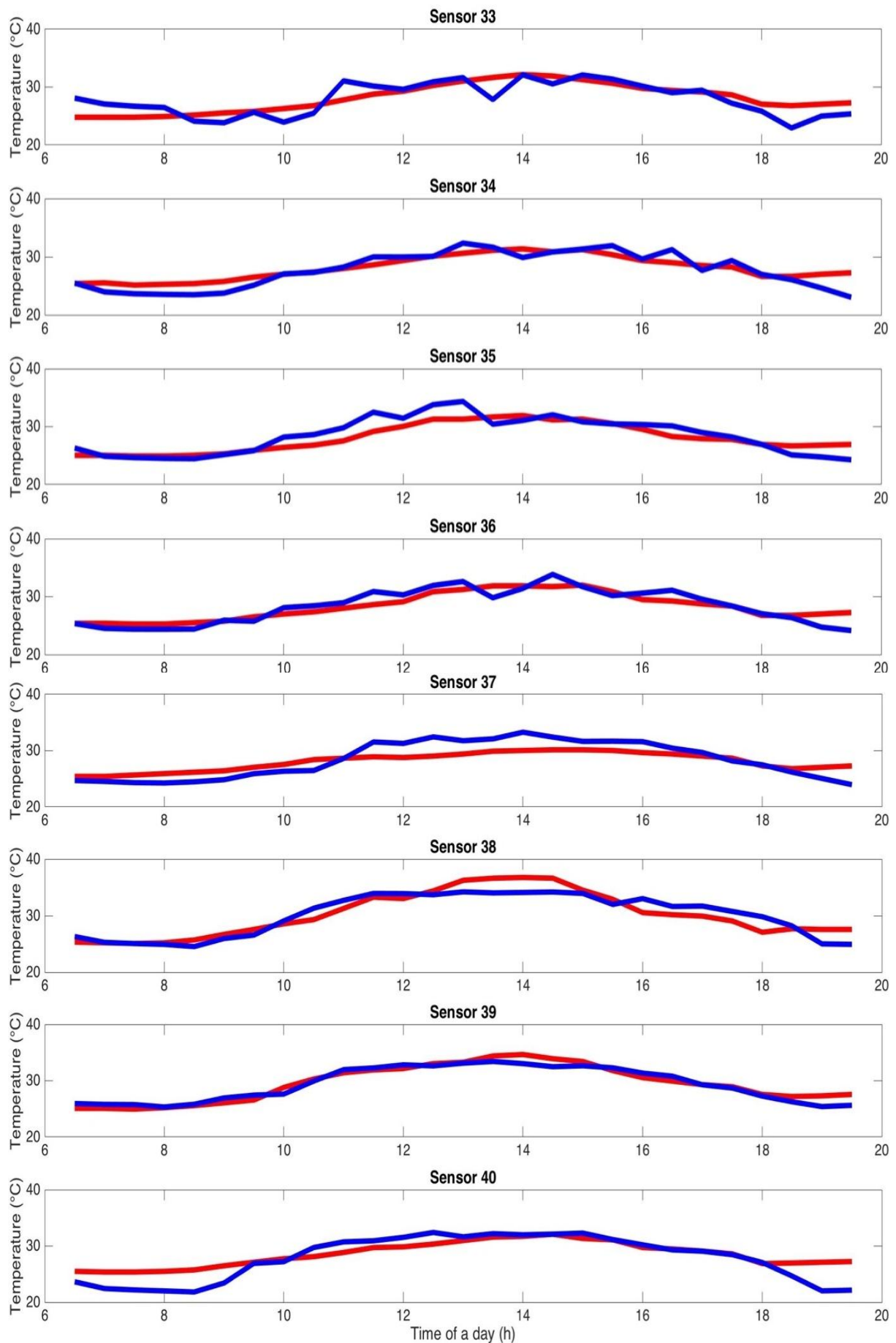
Figure8. *Validated air temperature at Sensors 17-24 against measured data. Legend: measured data (red line), simulated results (blue line).*

Figure9. *Validated air temperature at Sensors 25-32 against measured data. Legend: measured data (red line), simulated results (blue line).*

Figure10. *Validated air temperature at Sensors 23-40 against measured data. Legend: measured data (red line), simulated results (blue line).*
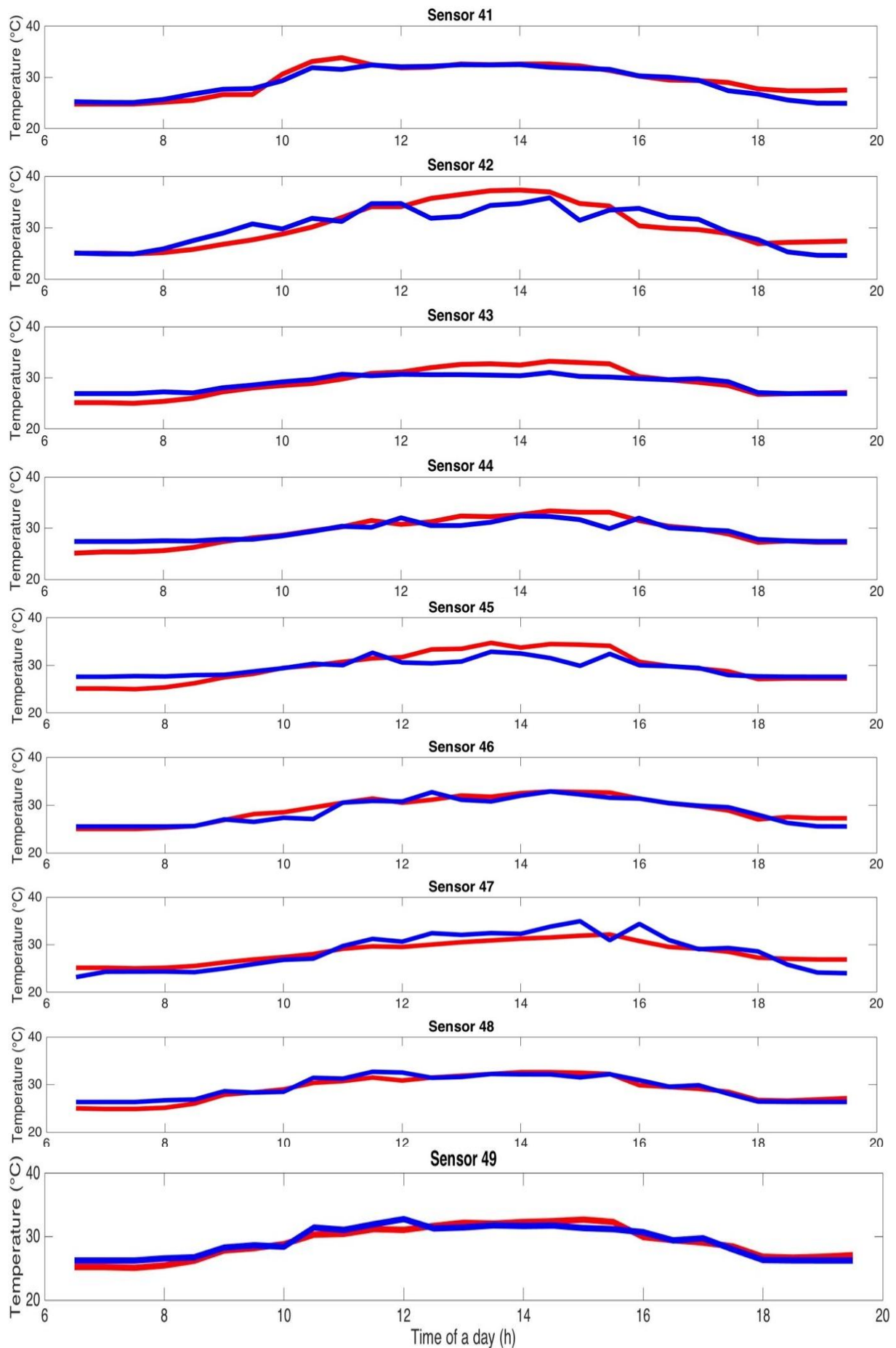
Figure11.*Validated air temperature at Sensors 41-49 against measured data. Legend: measured data (red line), simulated results (blue line).*

Table4. *Statistics of simulated air temperature at sensors 1-49.*

|	Sensor 1	Sensor 2	Sensor 3	Sensor 4	Sensor 5	Sensor 6	Sensor 7
r	0.96	0.94	0.93	0.91	0.89	0.87	0.89
MAE (%)	7.40	11.44	38.74	12.79	13.00	13.23	15.11
	Sensor 8	Sensor 9	Sensor 10	Sensor 11	Sensor 12	Sensor 13	Sensor 14
r	0.91	0.91	0.90	0.93	0.90	0.93	0.92
MAE (%)	13.67	15.38	11.29	9.87	12.49	10.03	12.90
	Sensor 15	Sensor 16	Sensor 17	Sensor 18	Sensor 19	Sensor 20	Sensor 21
r	0.91	0.90	0.90	0.92	0.91	0.93	0.90
MAE (%)	14.57	14.30	67.37	64.49	74.33	58.00	47.06
	Sensor 22	Sensor 23	Sensor 24	Sensor 25	Sensor 26	Sensor 27	Sensor 28
r	0.90	0.72	0.89	0.90	0.90	0.93	0.91
MAE (%)	39.45	16.78	13.30	20.77	30.25	21.17	19.37
	Sensor 29	Sensor 30	Sensor 31	Sensor 32	Sensor 33	Sensor 34	Sensor 35
r	0.92	0.93	0.82	0.88	0.76	0.91	0.88
MAE (%)	11.37	9.82	21.36	14.11	20.12	17.83	17.41
	Sensor 36	Sensor 37	Sensor 38	Sensor 39	Sensor 40	Sensor 41	Sensor 42
r	0.90	0.93	0.91	0.96	0.92	0.93	0.86
MAE (%)	15.96	34.62	11.89	7.81	24.12	8.98	14.07
	Sensor 43	Sensor 44	Sensor 45	Sensor 46	Sensor 47	Sensor 48	Sensor 49
r	0.92	0.91	0.90	0.94	0.95	0.95	0.95
MAE (%)	13.83	11.36	14.16	9.41	20.69	9.05	9.69

RESULTS AND DISCUSSION

To quantify respective contributions from major heat sources and sinks to the urban thermal environment, impacts of air conditioners, traffic, grasslands and water bodies are discussed in this section as an implementation example of the developed simulation tool. Two scenarios of simulations are designed to achieve the goals, namely the base scenario where all regions are regarded as concrete and the real situation scenario where each region is set with the respective properties, such as buildings, road pavement, grasslands and water bodies as shown in Figure 1, respectively.

Impacts of Air Conditioners

In Singapore, the majority of installed air-conditioning systems on high rise residential buildings are split type air-conditioners, compact units rejecting heat from air-conditioning through a dry heat exchange. They affect and in turn exposed to the urban microclimate in their vicinity, with regard to capacity to provide cooling and the efficiency of their operation. Stack effect of split type air-conditioners on high rise buildings are induced by the buoyancy-driven airflow coming out from the condensing units with rejected heat. The increasingly hotter air accumulated at higher levels of the same building will reduce

the energy efficiency by increasing the ambient air temperature, the heat sink for the air-conditioners. The effect was confirmed in field measurements on Block H of Kent Vale buildings in Bruelisauer et al. (2014). The model uses the measurements of its case study to verify the tool.

The 24-storey Kent Vale Block H is chosen to study the stack effect of split type air-conditioners. The tool is forced by the real settings of initial air temperature and velocity of each split type air-conditioners on the north side of the Kent Vale Block H, as measured in Bruelisauer et al. (2014). The measurement of the stack effect was carried out on 23 November 2012. More details can be found in Bruelisauer (2014). Since the air-conditioners are located in the recessed area of Block H, horizontal wind is not considered in this simulation. The patterns of the simulated distributions of air temperature (Figure 12) match well the observed data in Bruelisauer et al. (2014). This indicates the tool is able to capture microclimatic effects induced by split type air-conditioners on high rise buildings, which ensures the capability in simulating impacts of building energy consumption as one of the heat sources in urban environment.
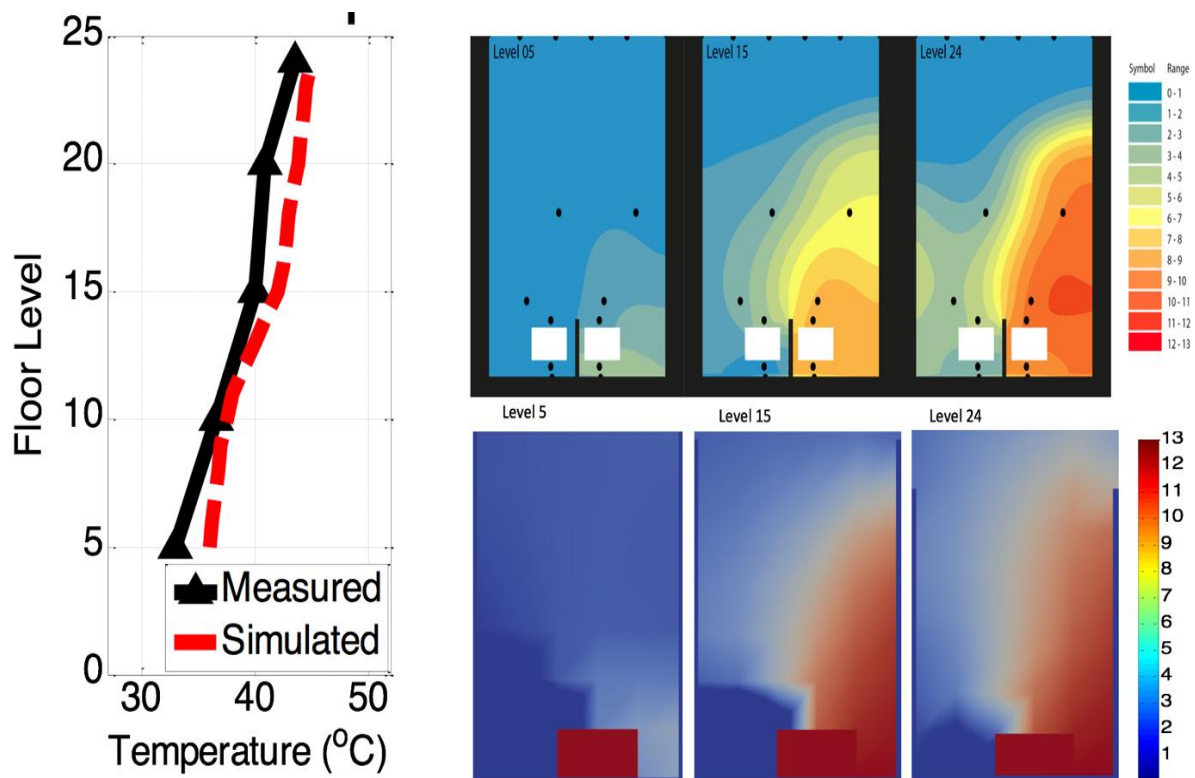
Figure12. *Validated simulated against measured data. Left: Validated vertical air temperature profile, indicating stack effect. Right: Horizontal air temperature distribution as temperature difference to ambient air temperature against measured data (top right image from Bruelisauer (2014)).*

Impacts of Traffic

Heat induced by traffic system in megacities is one of the major anthropogenic heat sources. Estimations of major anthropogenic heat flux includes building energy consumption, traffic system and human metabolism are made in Quah and Roth (2012). Time series of heat flux due to traffic system from 6am to 8pm during daytime (Figure 2) is adopted after part of Figure 3 in Quah and Roth (2012), which is employed as the forcing of traffic heat flux in the simulation tool.

Effects of traffic on urban heat island effect, or more specifically on the air temperature distribution patterns are identified by comparing the results of the base scenario where all regions are concrete with the real situation where each region is defined with its individual properties. Air temperature distribution patterns at height of 0.5m above ground at 9am, 1pm and 5pm are shown in Figure 13. 9 am is chosen as the morning situation the heat flux induced by traffic on Clementi Road is around 8.6 W/m2. 1pm represents the peak hour of solar radiation as observed and indicated in Xu (2016), when the traffic induced heat flux is around 14 W/ m2.

While 5pm stands for the afternoon situation and the corresponding heat flux on Clementi Road is set as 15 W/m2. Traffic induced heat flux starts to increase from 7am, peaks at around 1pm and remains until around 8pm before decreasing again.

It is found that the air temperature above Clementi Road is more than 2°C (up to 20 °C) higher than surrounding air throughout the daytime except during the early morning. Before 9am when the traffic is not heavy, the air temperature above Clementi Road is almost as the same as other concrete regions. As shown in Figure 13, it is also noticed that the heating effects of Clementi Road reaches beyond its upright regions and also heats up other parts such as the region beside Block I through convection. Due to radiation effects of the hot road surface of Clementi Road, gradually decreased heating effects are observed around the Clementi Road, especially towards Grassland 4 area. The interesting air temperature distribution pattern around three high-rise buildings and the verandah is decided the interactions between building geometries, solar radiation and surrounding cool air, which will be investigated in another separate study.
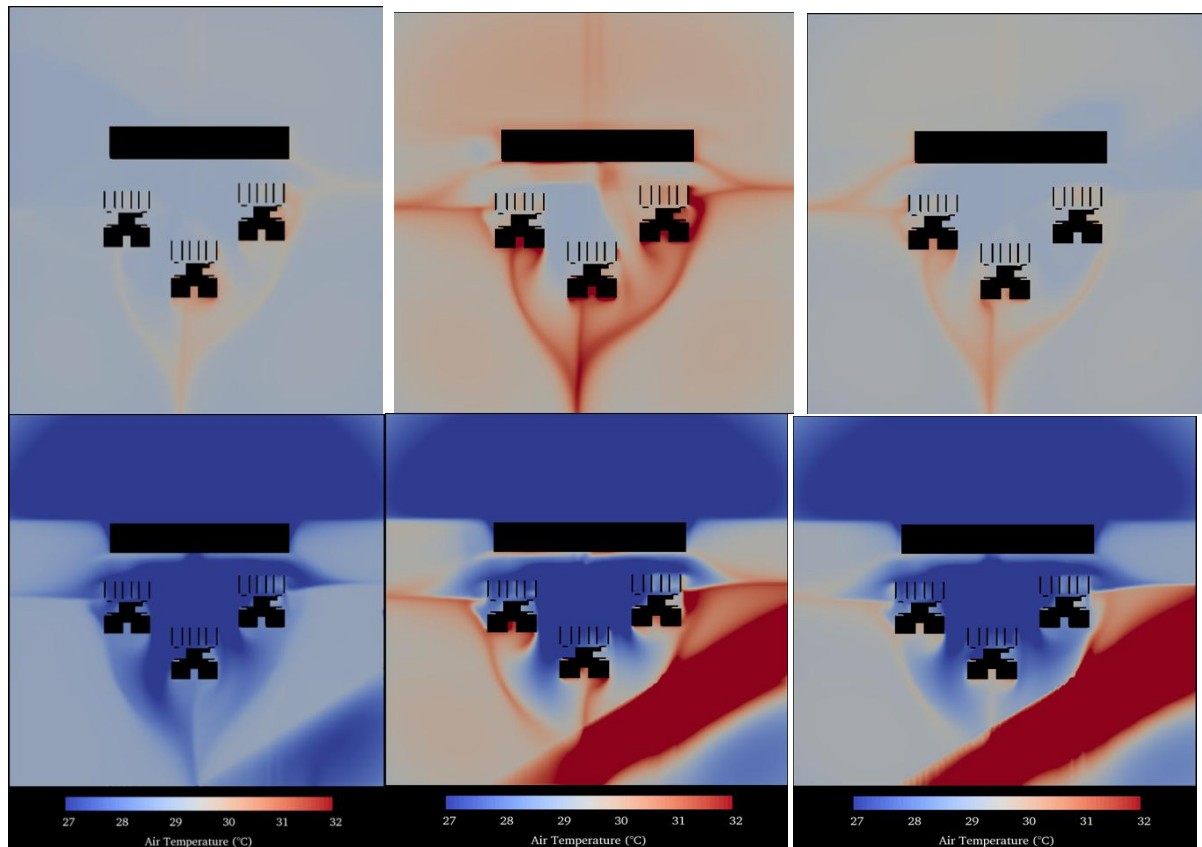
Figure13. *Air temperature distribution pattern at height of 0.5m above ground at 9am (left), 1pm (middle) and 5pm (right) when all regions are concrete (upper) and with respective properties (lower), respectively.*

Impacts of Grasslands

As illustrated in Figure 1, there are four grasslands in this model, namely Grasslands 1 and 2 at the ground level in between the three high-rise buildings and the verandah, Grassland 3 to the north of the verandah and Grassland 4 beside the Clementi Road located in the upper-left corner of the model domain. Cooling effects of grasslands are simulated by accounting for its evapotranspiration rate throughout the day with porous media technique of the region.

Both temporal and spatial effects of these four grasslands can be identified with Figure 13. It is found that the cooling effects of grasslands are quite consistent throughout the whole day. The distribution pattern of cooler zone is decided by the interactions of the cool air around grasslands, surrounding buildings and hotter air. Grasslands 1 and 2 is found to be able to cool down much larger area than their upright surface through intrusion into the hotter regions from gaps between three high-rise buildings and the verandah. The cooling effects of Grasslands 1 and 2 can be roughly estimated as 2°C, as read from Figure 6. Similar to Grasslands 1 and 2, Grasslands 3 is also found to cool down the surrounding environment by around 2°C.

Shading effects from the high-rise buildings could bring the air temperature by around 0.5°C, as can be observed in Figure 13. The cooling effects of shading is most significant at noon, which is around 1pm of Singapore time, as can be seen in Figure 13. Deducting the cooling effects of shading from the combined cooling effects above Grasslands 1 and 2, their real contributions are around 1.5°C. Due to the relatively smaller size, Grassland 4 is able to cool down the surrounding hot air by around 0.5 °C, which is the smallest among all four grasslands.

To quantify the cooling effects of grasslands along the vertical direction, air temperature distribution pattern at heights of 1m, 1.5m and 2m above ground at 1pm are plotted in Figure 14 for Scenarios 1 and 2, respectively. Combining with Figure 13, it is found that the cooling effects of grasslands can reach up to 2m above ground depends on their sizes. At the height of 2m above ground, Grasslands 1 and 2 can still cool down the surrounding hot air by more than 0.5°C. Figure 14 also indicates the cooling effects of shading from high-rise buildings does not change much throughout the day, as the simulation is carried out on 23 November when sun rises from Southeast and

sets in Southwest. On this specific day, the open space between three high-rise buildings and the verandah is located in the shadow throughout the daytime. The relatively cooler zone in the middle of the open space between Blocks G, H and I is mainly induced by the shading of Bridge H. Although the cooler zone above Grasslands 3

and 4 could also go up to 2m above the ground, the cooling effects are much smaller than those of Grasslands 1 and 2, especially combining with the shadings from the three high-rise buildings. While Grassland 3 still can cool down the hot air by less than 0.5°C, which is slighter stronger than that of Grassland 4.
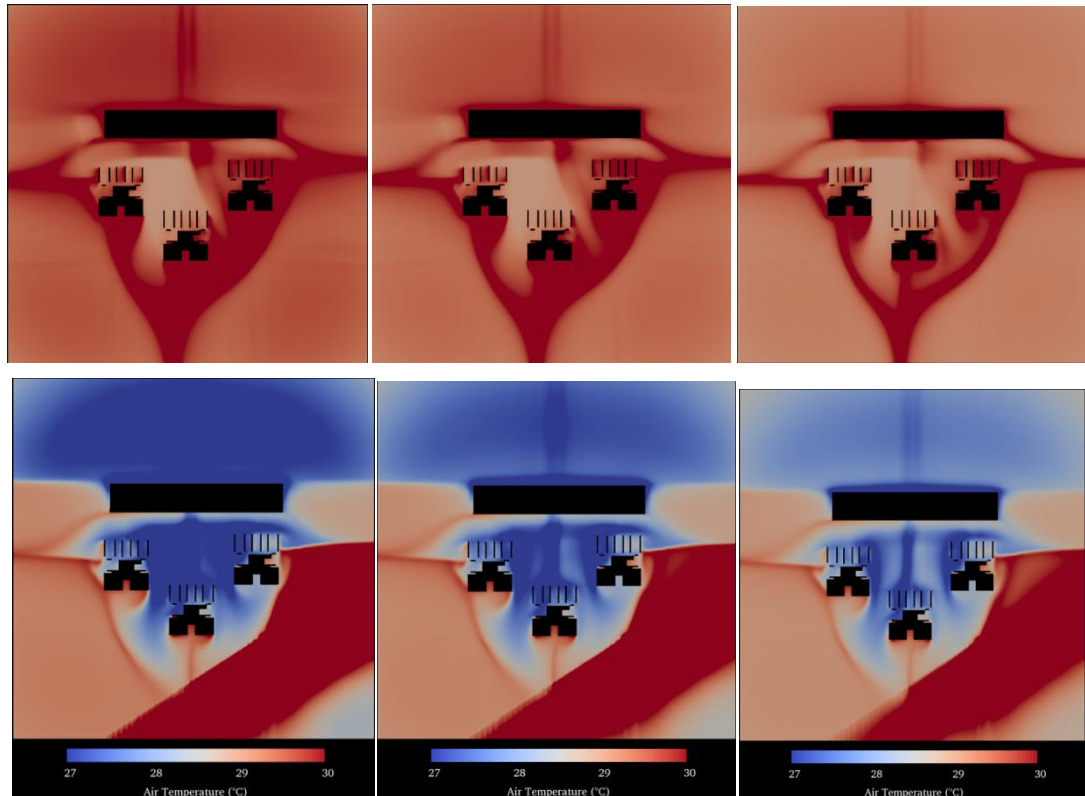
Figur14. Air temperature distribution pattern at heights of 1m (left), 1.5m (middle) and 2m (right) above ground at 1pm when all regions are concrete (upper) and with respective properties (lower), respectively.

Impacts of Water Bodies

Effects of water bodies on urban heat islands are identified by comparing air temperature distribution pattern above water surfaces with the situation that there is no water body. To simulate effects of water bodies on urban heat islands, evaporation rates of the water bodies in this model are set according to measured data. As illustrated in Figure 1, there are five water bodies in this model, namely Pools 1-4 located at the ground floor beside Grasslands 1 and 2, and the swimming pool at the top of the verandah. Due to relatively smaller sizes of the ground water feature pools, effects of water bodies on urban heat islands are mainly focused on the swimming pool. Since the swimming pool is at the top of the verandah, air temperature distribution pattern at heights of 7m, 7.5m and 8m at 1pm are plotted in Figure 15 for both scenarios.

It is found that the air temperature at the water surface of the swimming pool is around 1.5 °C cooler than the surrounding air, which is relatively smaller than the cooling capability of grasslands. The relatively cooler air can go up to 1m above the water surface with temperature of around 0.5°C lower than the surrounding air. In addition, the cooled down region above the water surface does not expand much through radiation, which is slightly weaker than that of grasslands. The possible reasons for difference in cooling capabilities between grasslands and water bodies can be mainly attributed to the fundamental difference between evaporation and evapotranspiration. Evaporation of water from water bodies in urban area is mainly induced by the heating effects of solar radiation. Since small water bodies have relatively weaker total amount of water evaporated during daytime than huge water bodies such as lakes and reservoirs. When the water bodies in urban area are moving such as running rivers and active coastal seas, the cooling effects due to

evaporation of water bodies will be much stronger than those of small water features such as swimming pools and landscape pools. While evapotranspiration of greenery includes grasslands and trees is the combined effect of both evaporation and transpiration. Due to photosynthesis activities of greenery when there is sufficient supply of sunlight, carbon dioxide, nitrogen and phosphorus, much cooler water vapor leaving the surfaces of leaves will enter the environment with initial momentum, which helps to magnify the cooling effects of greenery.

Other than cooling effects of water bodies, it is recommended to name the effects of water bodies as balancing effects, which will avoid the surrounding environment from being neither too hot nor too cold, as the specific heat capacity of water is 4.2 times that of air.

As shown in Figure 15, it is also found that the air temperature in the whole domain is slightly lower with the existence of grasslands and water bodies in the real situation than the base scenario where all regions are regarded as concrete. This combined cooling effect through interactions between major heat sources and sinks, and the surrounding air can be as high as around 1°C at critical locations around the buildings even at the height of 8m above the ground. Judging from Figure 15, the heating effects of Clementi Road can still weakly affect air temperature at the height of 8m above the ground.
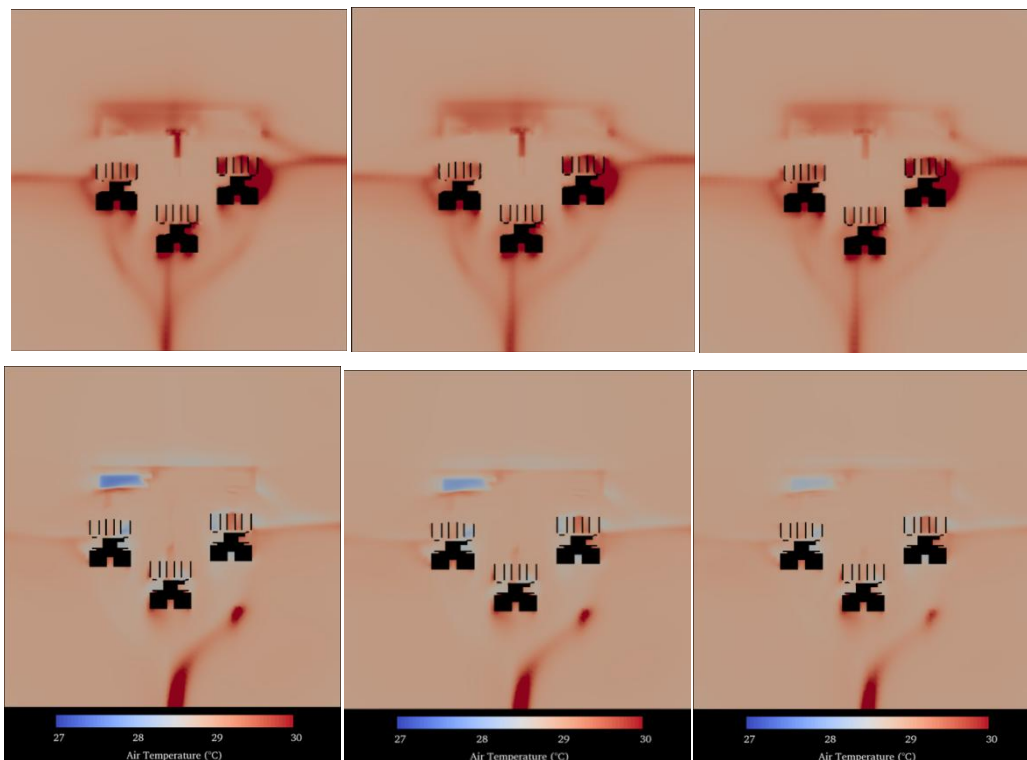
Figure15. *Air temperature distribution pattern at heights of 7m (left), 7.5m (middle) and 8m (right) above ground at 1pm when all regions are concrete (upper) and with respective properties (lower), respectively.*

CONCLUSIONS

An integrated urban heat island simulation tool is developed by accounting for major heat sources and heat sinks in selected area of interest, and their interactions with the surrounding environment. By comparing simulated solar radiation and air temperature on a typical day of each month throughout the whole year with observed data at Kent Vale buildings, it is found that the simulation tool could perform well in simulating solar radiation and air temperature. A second validation case at Punggol Waterway Terrace I further ensures the capability of the developed integrated urban heat island simulation toolin predicting air temperature distribution pattern across the model domain.

As an implementation example of the developed integrated urban heat island simulation tool, effects of traffic, grasslands and water bodies on urban heat islands are investigated in this study by comparing results from two different scenarios, following the simulation-aided design concept in Huang and Xu (2017). In Scenario 1, all regions are set as concrete, while in Scenario 2, each region is set as its own property. It is found that the air temperature above Clementi Road is more than 2°C and can be up to 20 °C

higher than surrounding air throughout the daytime except during the early morning. Before 9am when the traffic is not heavy, the air temperature above Clementi Road is almost as the same as other concrete regions. The heating up effects of Clementi Road also extends to surrounding area through radiation and can affect air temperature even at 8m above the ground.

Cooling effects of grasslands are found to be quite consistent throughout the whole day. The distribution pattern of cooler zone is decided by the interactions of the cool air around grasslands, surrounding buildings and hotter air. Grasslands is found to be able to cool down much larger area than their upright surface through intrusion into the hotter regions from gaps between three high-rise buildings and the verandah. The cooling effects of Grasslands can be roughly estimated as 2°C, with larger values for larger grasslands. It is also found that the cooling effects of grasslands can reach up to 2m above ground depends on their sizes.

The air temperature at the water surface of the swimming pool is found to be around 1.5 °C cooler than the surrounding air, which is relatively smaller than the cooling capability of grasslands. The relatively cooler air can go up to 1m above the water surface with temperature of around 0.5°C lower than the surrounding air. In addition, the cooled down region above the water surface does not expand much through radiation, which is slightly weaker than that of grasslands. The possible reasons for difference in cooling capabilities between grasslands and water bodies can be mainly attributed to the fundamental difference between evaporation and evapotranspiration. It is recommended to name the effects of water bodies on urban heat islands as balancing effects, which will avoid the surrounding environment from being neither too hot nor too cold.

By combing different urban heat islands mitigation strategies such as increase the greenery coverage with densely located grasslands and trees and have more suitable water bodies, better cooling effects can be achieved to improve the thermal environment in megacities. While such a combination of different mitigation strategies of urban heat island effect could be well evaluated by the developed integrated urban heat island simulation tool, as illustrated with the implementation example.

REFERENCES

[1] Allegrini, J. and Carmeliet, J., 2017. Simulations of local heat islands in Zurich with coupled CFD and building energy models. Urban Climate, in press. http://dx.doi.org/10.1016/j.uclim.2017.02.003.

[2] Allegrini, J., Dorer, V. and Carmeliet, J., 2015. Coupled CFD, radiation and building energy model for studying heat fluxes in an urban environment with generic building configurations. Sustainable Cities and Society, 19, 385-394.

[3] Bruelisauer, M., 2014. LowEx heat rejection systems in the tropics: Beyond energy efficiency, towards integrated multi-scale cooling system. Doctoral Thesis No. 22273, ETH Zurich.

[4] Bruelisauer, M., Meggers, F., Saber, E., Li, C. and Leibundgut, H., 2014. Stuck in a stack – Temperature measurement of the microclimate around split typecondensing units in a high rise building in Singapore. Energy and Buildings, 71, 28-37.

[5] Chen, Y. and Wong, N.H., 2006. Thermal Benefits of City Parks. Energy and Buildings, 38(2), 105–120.

[6] Chow, W.T.L. and Roth, M., 2006. Temporal Dynamics of the Urban Heat Island of Singapore. International Journal of Climatology, 26, 2243–2260.

[7] Chow, W.T.L., Salamanca, F., Georgescu, M., Mahalov, A., Milne, J.M. and Ruddell, B.L., 2014. A Multi-Method and Multi-Scale Approach for Estimating City-Wide Anthropogenic Heat Fluxes. Atmospheric Environment, 99, 64–76.

[8] Edwards, P.J., Hertig, T. and Sadlo, F., 2016. Proceedings of the 4th International Conference on Countermeasures to Urban Heat Island, Singapore.

[9] Fidaros, D., Baxevanou, C., Tsangrassoulis, A., Bartzanas, T. and Kittas, C., 2017. Bioclimatic Reformation of urban area – a CFD study. Procedia Environmental Science, 38, 586-594.

[10] Gao, Y., Xu, J., Yang, S., Tang, X., Zhou, Q., Ge, J., Xu, T. and Levinson, R., 2014. Cool Roofs in China: Policy Review, Building

Simulations, and Proof-of-Concept Experiments. Energy Policy, 74, 190–214.

[11] Gertland, L., 2008. Heat Islands: Understanding and Mitigating Heat in Urban Area. London: Earthscan.

[12] Giannaros, T.M., Melas, D., Daglis, I.A. and Keramitsoglou, I., 2014. Development of an operational modelling system for urban heat islands: an application to Athens, Greece. Natural Hazards and Earth System Sciences, 14, 347-358.

[13] Howell, J.R., Siegel, R. and Menguc, M.P., (2010). Thermal Radiation Heat Transfer. Fifth Edition. CRC Press.

[14] Huang, X. and Xu, M., 2017. Simulation Aided Design: Using "CFD simulation – design loop" for Better Thermal Environment. GSTF Journal of Engineering Technology, 4(3), 8pp.

[15] Jusuf, S.K., Wong, N.H., Hagen, E., Anggoro, R. and Hong, Y., 2007. The Influence of Land Use on the Urban Heat Island in Singapore. Habitat International, 31(2), 232–242.

[16] Li, X-X. and Norford, L.K., 2016. Evaluation of cool roof and vegetations in mitigating urban heat island in a tropical city, Singapore. Urban Climate, 16, 59-74.

[17] Li, X-X., Koh, T.Y., Entekhabi, D., Roth, M., Panda, J. and Norford, L.K., 2013. A Multi-Resolution Ensemble Study of a Tropical Urban Environment and Its Interactions with the Background Regional Atmosphere. Journal of Geophysical Research – Atmospheres, 118(17), 9804–9818.

[18] Mackey, C.W., Lee, X. and Smith, R.B., 2012. Remotely sensing the cooling effects of city scale efforts to reduce urban heat island. Building and Environment, 49, 348-358.

[19] Mirzaei, P.A., 2015. Recent challenges in modelling of urban heat island. Sustainable Cities and Society, 19, 200-206.

[20] Oke, T.R., 1973. City size and the urban heat island. Atmospheric Environment, 7(8), 769-779.

[21] Ooka, R., 2007. Recent development of assessment tools for urban climate and heat-island investigation especially based on experiences in Japan. International Journal of Climatology, 27, 1919-1930.

[22] Quah, A.K.L. and Roth, M., 2012. Diurnal and weekly variation of anthropogenic heat emissions in a tropical city, Singapore. Atmospheric Environment, 46, 92-103.

[23] Roth, M, and Chow, W., 2012. A Historical Review and Assessment of Urban Heat Island Research in Singapore. Singapore Journal of Tropical Geography, 33, 381–397.

[24] Saneinejad, S., Moonen, P., Defraeye, T., Derome, D. and Carmeliet, J., 2012. Coupled CFD, radiation and porous media transport model for evaluating evaporative cooling in an urban environment. Journal of Wind Engineering and Industrial Aerodynamics, 104-106, 455-463.

[25] Shaffer, S.R., Chow, W.T.L., Georgescu, M., Hyde, P., Jenerette, G.D., Mahalov, A., Moustaoui, M. and Ruddell, B.L., 2014. Multiscale Modeling and Evaluation of Urban Surface Energy Balance in the Phoenix Metropolitan Area. Journal of Applied Meteorology and Climatology, 54(2), 322–338.

[26] Sproul, J., Wan, M.P., Mandel, B.H. and Rosenfeld, A.H., 2014. Economic Comparison of White, Green, and Black Flat Roofs in the United States. Energy and Buildings, 71, 20–27.

[27] Tan, C.L., Tan, P.Y., Wong, N.H., Takasuna, H., Kudo, T., Takemasa, Y., Lim, C.V.J. and Chua, H.X.V., 2017. Energy and Buildings, in press, http://dx.doi.org/10.1016/j.enbuild.2017.01.011.

[28] Tominaga Y., Sato, Y. and Sadohara, S., 2015. CFD simulations of the effect of evaporative cooling from water bodies in a micro-scale urban environment: validation and application studies. Sustainable Cities and Society, 19, 259-270.

[29] Wong, N.H. and Chen, Y., 2006. Exploring the Urban Heat Island Effect in Singapore. In Tropical Sustainable Architecture, ed. Bay Joo Hwa and Ong Boon Lay, 10-1-10-23. London: Architectural Press, 23 pp.

[30] Xu, M., 2016. Towards a cooler Singapore. Global Journal of Science Frontier Research, 16(3), 32-35.

[31] Xu, M., Brülisauer, M. and Berger, M., 2017. Development of a new urban heat island modelling tool: Kent Vale case study. Procedia Computer Science, 108, 225-234.

[32] Xu, M., 2017. Impacts of Building Geometries and Radiation Properties on Urban Thermal Environment. Procedia Computer Science, 108, 2517-2521.